Clim Dyn (2013) 41:307–326
DOI 10.1007/s00382-012-1485-y

Diurnal and seasonal variations of wind farm impacts on land surface temperature over western Texas

Liming Zhou · Yuhong Tian · Somnath Baidya Roy · Yongjiu Dai · Haishan Chen

Received: 28 March 2012 / Accepted: 3 August 2012 / Published online: 24 August 2012

Abstract This paper analyzes seasonal and diurnal variations of MODerate resolution Imaging Spectroradiometer (MODIS) land surface temperature (LST) data at ~1.1 km for the period of 2003–2011 over a region in West-Central Texas, where four of the world's largest wind farms are located. Seasonal anomalies are created from MODIS Terra (~10:30 a.m. and 10:30 p.m. local solar time) and Aqua (~1:30 a.m. and 1:30 p.m. local solar time) LSTs, and their spatiotemporal variability is analyzed by comparing the LST changes between wind farm pixels (WFPs) and nearby non wind farm pixels (NNWFPs) using different methods under different quality controls. Our analyses show consistently that there is a warming effect of 0.31–0.70 °C at nighttime for the nine-year period during which data was collected over WFPs relative to NNWFPs, in all seasons for both Terra and Aqua measurements, while the changes at daytime are much noisier. The nighttime warming effect is much larger in summer than winter and at ~10:30 p.m. than ~1:30 a.m. and hence the largest warming effect is observed at ~10:30 p.m. in summer. The spatial pattern and magnitude of this warming effect couple very well with the geographic distribution of wind turbines and such coupling is stronger at nighttime than daytime and in summer than winter. Together, these results suggest that the warming effect observed in MODIS over wind farms are very likely attributable to the development of wind farms. This inference is consistent with the increasing number of operational wind turbines with time during the study period, the diurnal and seasonal variations in the frequency of wind speed and direction distribution, and the changes in near-surface atmospheric boundary layer (ABL) conditions due to wind farm operations. The nocturnal ABL is typically stable and much thinner than the daytime ABL and hence the turbine enhanced vertical mixing produces a stronger nighttime effect. The stronger wind speed and the higher frequency of the wind speed within the optimal power generation range in summer than winter and at nighttime than daytime likely drives wind turbines to generate more electricity and turbulence and consequently results in the strongest warming effect at nighttime in summer. Similarly, the stronger wind speed and the higher frequency of optimal wind speed at ~10:30 p.m. than that at ~1:30 a.m. might help explain, to some extent, why the nighttime LST warming effect is slightly larger at ~10:30 p.m. than ~1:30 a.m. The nighttime warming effect seen in spring and fall are smaller than that in summer and can be explained similarly.

L. Zhou (✉)
Department of Atmospheric and Environmental Sciences, University at Albany, State University of New York, 1400 Washington Avenue, Albany, NY 12222, USA
e-mail: lzhou@albany.edu

Y. Tian
IMSG at NOAA/NESDIS/STAR, Camp Springs, MD 20746, USA

S. Baidya Roy
Department of Atmospheric Sciences, University of Illinois, 105 South Gregory Street, Urbana, IL 61801, USA

Y. Dai
School of Geography, Beijing Normal University, Beijing 100875, China

H. Chen
Key Laboratory of Meteorological Disaster of Ministry of Education, Nanjing University of Information Science and Technology, Nanjing 210044, China

Keywords Wind farm · Impacts on weather and climate · Land surface temperature · Land cover land use · MODIS · West-Central Texas

1 Introduction

Wind energy is among the world's fastest growing sources of energy. Through the end of 2011, the US wind industry has installed a total of 46,919 megawatts (MW) of capacity, making it second in the world behind China (AWEA 2012). The installation of 6,810 MW during 2011 increased by 31 % from the 2010 total installations and there are over 8,300 MW currently under construction involving over 100 separate projects spanning 31 states plus Puerto Rico (AWEA 2012). While providing a clean source of electricity, the US wind industry generates tens of thousands of jobs and billions of dollars of economic activity and these numbers are expected to increase significantly in the future (USDOE 2011). Even though current US wind power penetration is only about 2.3 % of all electric generation capacity (AWEA 2011), the US Department of Energy envisions that wind power could supply 20 % of all US electricity by 2030 (USDOE 2008).

Wind turbines convert wind's kinetic energy into electricity with their typically two or three propeller-like blades around a rotor. They modify surface-atmosphere exchanges and transfer of energy, momentum, mass and moisture within the atmosphere by increasing surface roughness, changing atmospheric boundary layer stability and enhancing turbulence in the rotor wakes (Knippertz et al. 2000; Simmonds and Keay 2002; Baidya Roy and Traiteur 2010; Baidya Roy 2011). These changes, if spatially large enough, may have noticeable impacts on local to regional weather and climate. Given the current installed capacity and the projected installation across the world (AWEA 2011, 2012), wind farms are likely becoming a major driver of manmade land use change on Earth. Hence, understanding wind farm interactions with the atmosphere and assessing their potential impacts are of significant societal importance.

Recent studies have investigated the possible impacts of wind farms on local to global weather and climate. Although debates exist regarding the regional to global-scale effects (Keith et al. 2004; Kirk-Davidoff and Keith 2008; Sta Maria and Jacobson 2009; Barrie and Kirk-Davidoff 2010; Wang and Prinn 2010), modeling studies agree that wind farms can significantly affect local-scale meteorology (Baidya Roy et al. 2004; Adams and Keith 2007; Baidya Roy and Traiteur 2010; Baidya Roy 2011; Fiedler and Bukovsky 2011). However, these studies are based primarily on numerical simulations of regional and global models, which due to lack of observations, crudely represent the effects of wind turbines by explicitly increasing either surface roughness length or turbulence kinetic energy. Evidently, more realistic model parameterizations should be developed and modeling results should be validated against the observations.

Unfortunately information on meteorological variables in and around wind farms is not readily available in the public domain. Till date only one study has investigated the impacts of wind farms on surface temperatures using observed data on near-surface air temperatures from an operational wind farm in California (Baidya Roy and Traiteur 2010). They found a warming effect at night and a cooling effect at daytime in the wake region of the wind farm. However, the geography of this wind farm is unique because it is located at the mouth of San Gorgonio pass just north of the city of Palm Springs. It is difficult to filter out urban and topographic effects and extrapolate these results into broad conclusions about the impacts of wind farms. Additionally, the observed data are only from two meteorological towers for 1.5 months. Hence more observational evidence of wind farm effects at larger scales and longer periods is needed, particularly over the Midwest and the Great Plains where wind farm growth rate is among the highest in the US.

The best way to estimate the impacts of wind farms will be to conduct extensive but likely expensive field campaigns. Another cost-efficient option is to identify impacts of wind farms over a wider range of spatiotemporal scales using remote sensing data. Most importantly, the knowledge obtained from the impact studies will also provide guidance to future field campaign organizers about the optimal selection and deployment of instruments and the optimal location and timing of planned field campaigns. Satellites provide information of global spatial sampling at regular temporal intervals and thus have the potential to monitor and detect impacts of large wind farms with spatial detail. Zhou et al. (2012) present the first observational evidence for likely impacts of large wind farms in West-Central Texas using satellite derived land surface temperature (LST) from MODerate resolution Imaging Spectroradiometer (MODIS). They found a nighttime warming effect over wind farms relative to nearby non wind farm regions and attribute this warming primarily to wind farms because its spatial pattern and magnitude couples very well with the geographic distribution of wind turbines.

Zhou et al. (2012) only analyzed MODIS LST in two seasons (winter and summer) and combined MODIS data into one daytime and one nighttime LST for the period 2003–2011. The present paper furthers the work of Zhou et al. (2012) to examine seasonal and diurnal variations of likely wind farm impacts by analyzing MODIS LST at four

measuring times (twice in daytime and twice in nighttime) for all seasons under different quality controls.

2 Data and methods

2.1 Study region

Texas has the most installed wind power capacity of any US state, with 10,377 MW of installation through the end of 2011, which accounts for about 22 % of the US total wind industry (46,919 MW) during the same period (AWEA 2012). There are many big wind farms in Texas. West-Central Texas represents the state's largest concentration of wind farms and the most active deployment and operations center for wind energy and continues to experience rapid growth (Combs 2008a). Here we focus our study on a region (32.1°N–32.9°N, 101°W–99.8°W) (Figs. 1, 2) in West-Central Texas that is home to four of the world's largest wind projects and also to the largest single wind farm in the world (Combs 2008a). This region covers the entire Nolan County and part of Fisher, Scurry, Mitchell and Taylor Counties in Texas, with a total area of ~10,005 km^2 (~112.8 km × ~88.7 km).

2.2 Geographic location of wind turbines

We use the database of Obstruction Evaluation/Airport Airspace Analysis (OE/AAA) at Federal Aviation Administration (FAA) (https://oeaaa.faa.gov/oeaaa/external/portal.jsp) to identify wind farms and their geographic locations. To promote air safety and the efficient use of the navigable airspace, FAA requires any organization, who plans to sponsor any construction or alterations that may affect navigable airspace, to file a Notice of Proposed Construction or Alteration. FAA has the detailed record for each wind turbine built, altered or proposed in the period of 1988–2011. We download all cases processed by FAA during the entire period and identify only those wind turbines that have already been built in our study region based on their locations (latitude and longitude). In total, there are 2,358 wind turbines built as of November 17, 2011 (Figs. 1, 2a), most of which were built in 2005–2008, with ~90 % completed with construction by the end of 2008.

We verify the existence of these wind farms (Fig. 2b) using Google Earth where individual wind turbines can be seen clearly and identified. Given the large number of turbines located in our study region, it is impossible to precisely read the geographic location of each turbine site manually. Instead, we draw the boundary along the outside layer of wind turbines for each wind farm (Fig. 2b), which is very similar to Fig. 2a.

2.3 MODIS data

We use Collection 5 MODIS LSTs downloaded from (https://lpdaac.usgs.gov/get_data). MODIS is a key scientific instrument launched into Earth orbit by NASA in 1999 on board the Terra (EOS AM) satellite, and in 2002 on board the Aqua (EOS PM) satellite (http://modis.gsfc.nasa.gov/). The instruments (Terra and Aqua) orbit around the Earth, imaging the entire Earth's surface every 1–2 days and acquiring data in 36 spectral bands ranging in wavelength from 0.4 to 14.4 μm and at varying spatial resolutions. They pass across the equator at local solar time ~10:30 p.m. (Terra) and ~1:30 a.m. (Aqua) during

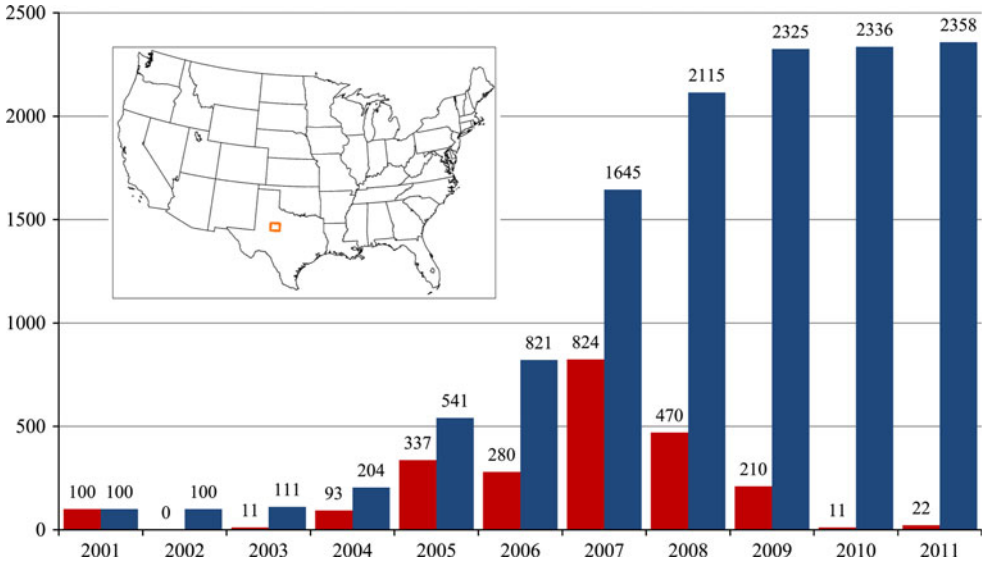

Fig. 1 Histograms of individual wind turbines built annually for the period 2001–2011 based on the data from FAA. The number of annual (*red*) and accumulated (*blue*) turbines built for each year is listed on the top of *each bar*. The location of the study region is *plotted* within the map of continental US

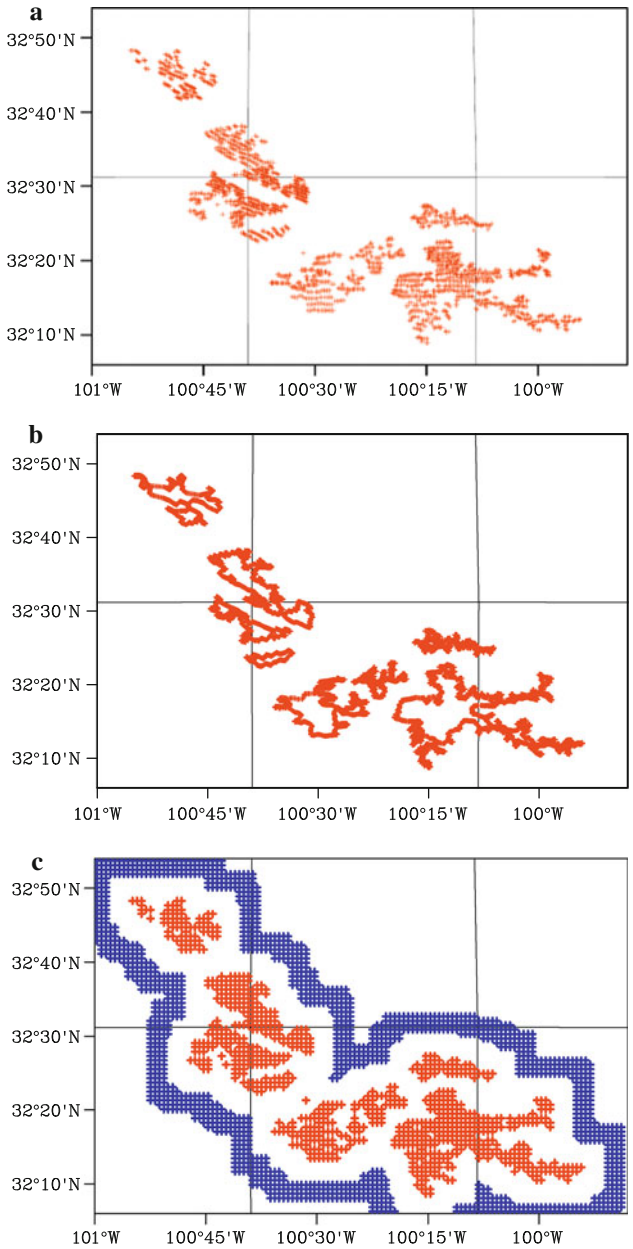

Fig. 2 Geographic locations (latitude and longitude) of wind turbines: **a** 2,358 individual turbine sites (*plus symbol* in *red*) built in the period 2001–2011 based on the FAA record, **b** the boundary of wind farms (*plus symbol* in *red*) identified via Google Earth, and **c** definition of wind farm pixels (WFPs, in *red*) and nearby non wind farm pixels (NNWFPs, in *blue*) at 0.01° resolution. In **b**, the outside layer of wind turbines were drawn in Google Earth as the boundary of wind farms. In **c**, pixels with at least one wind turbine are defined as WFPs (in total: 890 pixels) and those that are between 6 and 9 pixels (4 pixels in width) away from WFPs are defined as NNWFPs (in total: 1,538 pixels). The pixels between WFPs and NNWFPs (about 5 pixels between *red* and *blue*) are defined as the transitional zone given the difficulty in objectively defining the boundary of downwind impacts of wind farms

nighttime and ~10:30 a.m. (Terra) and ~1:30 p.m. (Aqua) during daytime, providing validated, global measurements in large-scale dynamics and processes occurring on the land, in the oceans, and in the lower atmosphere. For simplicity, we use local solar time ~22:30, ~1:30, ~10:30 and ~13:30 to denote the acquisition times of the MODIS LST measurements in this paper.

As LST changes diurnally, we include the MODIS data from both instruments (Terra and Aqua). Daily LST data are also available but with many gaps and missing values. Hence we choose 8-day LST products from Terra (MOD11A2) and Aqua (MYD11A2) that are averaged from 2 to 8 days of the daily product (Wan 2002). The MODIS LST data represent the best quality retrieval possible from clear-sky conditions over each 8-day period. Their accuracy has been assessed over a widely distributed set of locations and time periods via several ground-truth and validation efforts. Although there may be other improvements, these data have been used extensively in a variety of areas and proven to be of high quality. For example, validation studies in 47 clear-sky cases indicate that the accuracy of MODIS LST is better than 1 K in most cases (39 out of 47) and the root of mean squares of differences is less than 0.7 K for all 47 cases or 0.5 K for all but the 8 cases apparently with heavy aerosol loadings (Wan 2006).

For each year, there are 184 LST images (46 8-day composites × 4 times per composite). First, we aggregate the 8-day MODIS LST data into monthly means from the 8-day composites within each month and then create monthly anomalies by removing the monthly climatology for each pixel. Second, we aggregate the monthly means and anomalies into seasonal ones in DJF (Dec–Jan–Feb), MAM (Mar–Apr–May), JJA (Jun–Jul–Aug) and SON (Sep–Oct–Nov). Similarly, annual (referred to as ANN) means and anomalies are also created. As the Aqua data is only available starting in July 2002 while Terra has data starting in March 2000, we have in total 9 years of seasonal means and anomalies of LST for the period 2003–2011 (note that only the data with a whole year of LST are considered). Finally for each season in each year, we have 4 images of LST corresponding to the 4 acquisition times of the MODIS data.

The MODIS data are archived by tile (each tile represents a 10° by 10° grid cell) in the Sinusoidal equal area projection, which has a tilt angle of ~45° relative to the local latitude/longitude of our study region. So the MODIS seasonal mean and anomalies are re-projected into pixels at 0.01° resolution (~1.1 km), which is slightly coarser than the original MODIS 1 km data to avoid gaps in spatial interpolation. In total, there are 9,600 pixels (120 columns × 80 lines) centered around 2,358 wind turbines in the study region (Fig. 2).

For brevity, we use the following acronyms to represent two groups of pixels in our study region (Fig. 2c): (1) WFPs (wind farm pixels, i.e., 890) and (2) NNWFPs (nearby non-

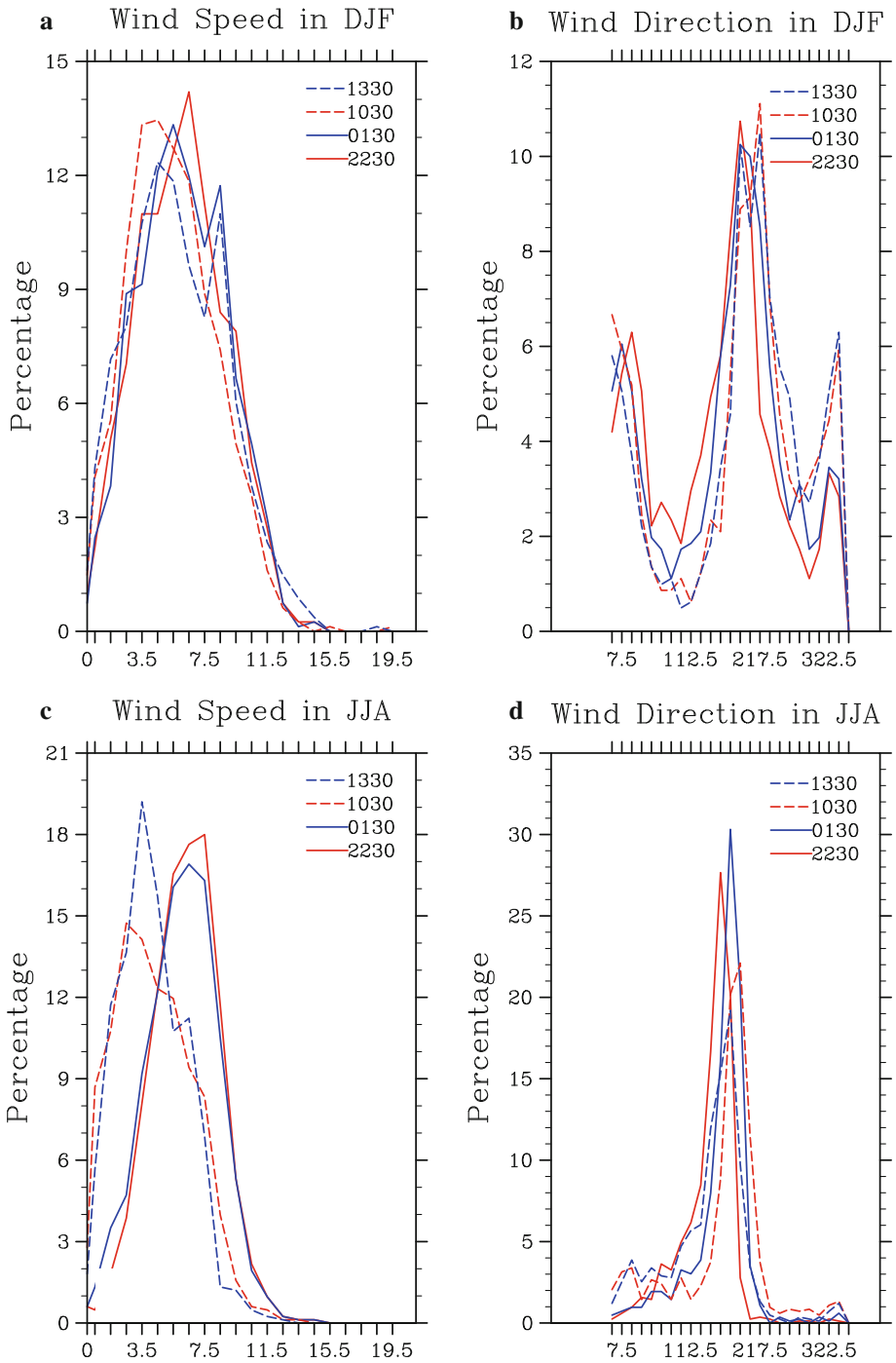

Fig. 3 Histogram of MERRA hourly 50 m wind speed (m/s) and direction in DJF (**a**, **b**) and JJA (**c**, **d**) averaged over the study region for the period of 2003–2011. Wind direction is determined by the direction from which it originates. It is measured in terms of degrees clockwise between 0 and 360 (°). The wind from North corresponds to 360°, East to 90°, South to 180° and West to 270°

wind-farm pixels, i.e., 1,538). We define the pixels with at least one wind turbine as WFPs and those that are between 6 and 9 pixels (4 pixels in width) away from WFPs as NNWFPs. We leave a transitional zone of 5 pixels between WFPs and NNWFPs given the difficulty in objectively defining the boundary of downwind pixels (Fig. 2c).

Quality assurance value (QA) fields are attached to the MODIS LST data (Table 1). QA can tell us whether the LST is produced ($QA_{01} = 00$ or 01) or not ($QA_{01} = 10$ or 11, due to cloud effects or other factors). If the LST is produced, the QA labels it into "good quality" ($QA_{01} = 00$) or "other quality" ($QA_{01} = 01$). For the LST produced from "other quality", its average error is provided ($QA_{67} = 00$ for errors $\leq$1 K, $QA_{67} = 01$ for errors $\leq$2 K, $QA_{67} = 10$ for errors $\leq$3 K and $QA_{67} = 11$ for errors >3 K).

To assess uncertainties of MODIS LST retrievals to our results, we consider four different QA controls: QA0

Table 1 Bit flags defined for quality assurance (QA) value in MODIS LST data

Acronyms QA type	Bits	Long name	Key
QA_{01}	1 & 0	Mandatory QA flags	00 = LST produced, good quality, not necessary to examine more detailed QA
			01 = LST produced, other quality, recommend examination of more detailed QA
			10 = LST not produced due to cloud effects
			11 = LST not produced primarily due to reasons other than cloud (such as ocean grid, grid not covered by all processed granules)
QA_{23}	3 & 2	Data quality flag	00 = good data quality
			01 = LST affected by thin cirrus and/or sub-pixel clouds
			10 = not processed due to missing pixels
			11 = not processed due to poor quality
QA_{45}	5 & 4	Emissivity error flag	00 = average emissivity error $\leq$ 0.01
			01 = average emissivity error $\leq$ 0.02
			10 = average emissivity error $\leq$ 0.04
			11 = average emissivity error $>$ 0.04
QA_{67}	7 & 6	LST error flag	00 = average LST error $\leq$ 1 K
			01 = average LST error $\leq$ 2 K
			10 = average LST error $\leq$ 3 K
			11 = average LST error $>$ 3 K

(QA_{01} = 00 & 01, i.e., LST produced from both "good quality" and "other quality"), QA1 (QA_{01} = 00, i.e., only those QA0 pixels labeled as "good quality"), QA2 (QA_{01} = 00 & 01 and QA_{67} = 00, i.e., only those QA0 pixels with LST errors $\leq$1 K) and QA3 (QA_{01} = 00 & 01 and QA_{67} = 01, i.e., only those QA0 pixels with LST errors $\leq$2 K). Obviously, QA1, QA2 and QA3 are a subset of QA0, with QA1 representing the fewest pixels with the best quality and QA0 the most pixels with all LST retrievals (except those not produced due to cloud effects and other factors). For a given region, we calculate the total number of pixels, P_0, and also the total number of pixels with LST retrievals for each QA control, P_i, (i = 0, 1, 2, 3), where the subscript i denotes QA0 to QA3. The value of $100*P_i/P_0$ is used to represent the percentage of LST retrievals (Table 2). For example, 60 % for QA0 means that 60 % of P_0 are produced with "good quality" and "other quality" (or 40 % of P_0 are not produced); 60 % for QA1 indicates that 60 % of P_0 are produced with "good quality".

As our analysis consist of four seasons plus ANN, four measuring times and four QA controls, it is impossible to plot all the results. Here we show primarily some of the results for QA0 in DJF and JJA in figures while the others are listed in tables. DJF and JJA are chosen to represent cold winter and hot summer while spring and fall are basically transitional seasons. QA0 is chosen for the purpose of visualization at the pixel level as excluding some "other quality" pixels from the LST images may result in some spatiotemporal gaps in the LSTs for QA1 to QA3.

2.4 Reanalysis wind data

We use the hourly wind data from Modern Era Retrospective-analysis for Research and Applications (MERRA) (Rienecker et al. 2011) for the period of 2003–2011 (Note that other reanalysis products also provide wind data but at 3-h or longer time scales). MERRA was developed to support NASA's Earth science objectives, by applying the state-of-the-art Global Modeling and Assimilation Office (GMAO/NASA) data assimilation system that includes many modern observing systems in a climate framework (Rienecker et al. 2011). The project focuses on historical analyses of the hydrological cycle on a broad range of weather and climate time scales and places the NASA EOS suite of observations (including MODIS data) in a climate context. It provides 3D 6-h atmospheric analyses and 2D hourly diagnostics (e.g., atmospheric single-level diagnostics of time averaged U- and V-wind components) at spatial resolution of 1/2° latitude × 2/3° longitude. Hourly winds of the MERRA data at 50 m above the surface are downloaded from http://disc.sci.gsfc.nasa.gov/ and re-projected into our study region at 0.01° resolution using nearest neighborhood interpolation. Seasonal wind climatology is created to identify downwind directions of wind farms and to understand the statistics of wind speed and direction (Table 3 and Fig. 3). MERRA also has winds at 5 m and 10 m above the surface but the wind at 50 m is chosen as it represents the turbine hub-height wind speeds better than the other levels. The reanalysis is provided at 0:30, 1:30, …, 23:30 UTC (Coordinated Universal Time).

Table 2 Percentage of MODIS LST retrievals for WFPs and NNWFPs (in parenthesis) under different QA controls for the period of 2003–2011

QA type[a]	Season	Nighttime		Daytime	
		~22:30	~01:30	~10:30	~13:30
QA0	DJF	98.86 (98.82)	97.53 (97.70)	96.31 (96.30)	98.76 (98.83)
	MAM	99.86 (99.68)	99.91 (99.84)	98.03 (98.56)	99.77 (99.94)
	JJA	99.44 (99.38)	93.87 (93.66)	98.33 (98.00)	92.53 (92.11)
	SON	99.31 (99.14)	99.54 (99.36)	98.28 (98.24)	99.28 (99.24)
	ANN	99.28 (99.17)	97.66 (97.56)	97.69 (97.71)	97.54 (97.45)
QA1	DJF	66.04 (69.58)	64.14 (67.56)	64.48 (65.69)	64.67 (66.74)
	MAM	70.40 (74.06)	68.29 (73.33)	67.37 (70.93)	66.93 (70.94)
	JJA	68.64 (73.12)	49.28 (47.69)	64.67 (68.50)	37.02 (37.92)
	SON	67.93 (71.60)	66.86 (70.87)	65.59 (67.05)	62.41 (66.73)
	ANN	68.07 (71.94)	61.88 (64.54)	65.51 (67.93)	57.50 (60.24)
QA2	DJF	86.93 (86.06)	81.60 (81.61)	79.29 (77.32)	81.60 (79.90)
	MAM	94.63 (93.87)	91.03 (92.71)	89.18 (88.64)	88.42 (89.04)
	JJA	92.54 (92.83)	63.59 (59.53)	86.81 (87.04)	46.10 (46.22)
	SON	91.36 (90.42)	88.94 (88.57)	87.49 (84.96)	82.46 (83.25)
	ANN	91.13 (90.60)	80.89 (80.15)	85.59 (84.30)	74.18 (74.07)
QA3	DJF	98.86 (98.82)	97.53 (97.70)	96.31 (96.30)	98.74 (98.83)
	MAM	99.86 (99.68)	99.91 (99.84)	98.03 (98.56)	99.77 (99.94)
	JJA	99.44 (99.38)	93.48 (93.38)	98.32 (98.00)	92.20 (91.88)
	SON	99.31 (99.14)	99.54 (99.36)	98.28 (98.24)	99.28 (99.24)
	ANN	99.28 (99.17)	97.56 (97.48)	97.69 (97.71)	97.45 (97.39)

WFPs and NNWFPs are defined in Fig. 2c; the percentage is calculated as the total number of retrieved LST pixels divided by the total number of pixels over WFPs and NNWFPs, respectively

[a] QA types are defined as QA0 ($QA_{01} = 00$ and 01), QA1 ($QA_{01} = 00$), QA2 ($QA_{01} = 00$ & 01 and $QA_{67} = 00$), and QA3 ($QA_{01} = 00$ & 01 and $QA_{67} = 01$), where QA_{01} and QA_{67} are defined in Table 1

We use the winds at 04:30, 07:30, 16:30 and 19:30 UTC, which roughly correspond to the MODIS LSTs at local solar time ~22:30, ~1:30, ~10:30 and ~13:30, for this analysis.

2.5 Detection and attribution methods

We first discuss the spatiotemporal variability of LST in the study region and next describe methods used to attribute and quantify the impacts of wind farms on LST.

2.5.1 LST spatiotemporal variability

Besides possible impacts from wind farms, LST variability over the study region consists of two major components: (1) temporal variability controlled primarily by regional or large-scale meteorological conditions and (2) spatial variability at pixel level that is mostly related to changes in topography and land surface types. Minimizing such variability is the key to uncovering wind farm impacts.

Figure 4 shows interannual variations of regional mean MODIS LST anomalies in DJF and JJA averaged over the entire study region for the period 2003–2011. The study region exhibits a strong interannual variability, particularly in summer. For example, in JJA, the LST ranges from −6.0 to 8.8 °C (−1.2 to 3.3 °C) at ~1:30 (~13:30), with the coldest year in 2007 and the warmest year in 2011 when the historic Texas drought occurred (Hylton 2011). The two measurements at daytime or nighttime generally show similar LST variations. For each season and each measuring time, we calculated this regional mean LST anomaly (i.e., one value per year from 2003 to 2011) and refer to it as the "regional interannual variability" thereafter.

MODIS LST also exhibits strong spatial variability at pixel level that is mostly related to changes in topography and land surface types (Zhou et al. 2012). Figure 5 shows the climatology of JJA LST at ~1:30 and ~13:30. The northeastern and southwestern parts of the study region are generally warmer than the southeastern and northwestern parts. The LST varies from one wind farm to another, within WFPs, and between WFPs and NNWFPs. Interestingly, the areal mean LST between WFPs and NNWFPs, however, is very small (Table 4), indicating the LSTs averaged over the two regions are very similar.

Table 3 Seasonal statistics of climatological MERRA 50-m winds for the period 2003–2011

Season	Nighttime		Daytime	
	22:30	1:30	10:30	13:30
Mean and standard deviation (in parenthesis) of wind speed (m/s)[a]				
DJF	6.99 (2.83)	7.07 (2.84)	6.38 (2.86)	6.70 (3.14)
MAM	8.19 (2.80)	7.80 (2.77)	6.88 (2.87)	6.88 (2.92)
JJA	7.27 (2.16)	7.02 (2.33)	5.15 (2.54)	5.08 (2.23)
SON	7.17 (2.48)	7.01 (2.62)	5.92 (2.83)	5.95 (2.89)
ANN	7.41 (2.62)	7.23 (2.66)	6.08 (2.85)	6.15 (2.90)
Percentage of wind speed of 7–9 m/s and 6–10 m/s (in parenthesis)[a]				
DJF	25.43 (46.42)	22.10 (47.16)	20.74 (40.86)	17.90 (40.74)
MAM	24.88 (46.26)	25.97 (50.97)	24.64 (47.10)	24.88 (46.38)
JJA	35.63 (63.89)	33.21 (59.78)	17.75 (33.70)	18.12 (30.19)
SON	29.30 (54.82)	27.96 (52.63)	20.39 (40.54)	17.83 (38.58)
ANN	28.83 (52.88)	27.34 (52.66)	20.88 (40.55)	19.70 (38.96)
Percentage of zonal wind within an angle $\pm 7.5°$ and $\pm 15°$ (in parenthesis)[b]				
DJF	5.19 (10.12)	4.07 (8.77)	5.06 (9.51)	6.79 (12.59)
MAM	4.11 (10.14)	4.35 (8.94)	4.47 (9.30)	5.56 (10.14)
JJA	2.90 (6.88)	1.57 (3.86)	3.50 (5.31)	3.14 (5.92)
SON	2.56 (7.81)	3.17 (5.86)	3.79 (8.06)	4.40 (8.79)
ANN	3.68 (8.74)	3.29 (6.85)	4.20 (8.04)	4.96 (9.35)

MERRA winds at 4:30, 7:30, 16:30 and 19:30 UTC are used to represent the wind speed of the MODIS four measurement times at local time ~22:30, ~01:30, ~10:30, and ~13:30, respectively

[a] Wind speed is calculated as $\sqrt{u^2 + v^2}$, where u and v represent the two wind components of the MERRA hourly data

[b] Wind direction is reported by the direction from which it originates and is measured in terms of degrees clockwise between 0° and 360°. The zonal wind with an angle $90 \pm 7.5°$ ($90 \pm 15°$) from East and $270 \pm 7.5°$ ($270 \pm 15°$) from West are used to estimate the frequency of zonal wind frequency within an angle of $\pm 7.5°$ ($\pm 15°$)

As the wind farm impact on LST is likely small in magnitude, our analysis attempts to isolate this impact from the background signal by minimizing the influence of topography, land cover, and regional interannual variations of weather/climate. Local effects at pixel level due to spatial variability in topography and land cover can be minimized through the use of anomalies as done in Sect. 2.3. The strong interannual variability can be minimized by removing the "regional interannual variability" from the original LST time series anomalies as introduced next.

2.5.2 *Spatial coupling analysis*

If the development of wind farms has some impacts on LST and if such impact is large enough to be detected by MODIS, the observed MODIS LST change should couple spatially with the wind turbines. Therefore, we calculate the LST difference between two periods (or two individual years) at pixel level, denoted as DLST, and check their spatial coupling with wind turbines (referred to as Method I). As wind turbines in the study region were constructed by stages, with most built in 2005–2008 (Fig. 1), we choose the first 3 years of data (2003–2005) to represent the case with the least impacts and the last 3 years (2009–2011) of data to represent the case with the most likely impacts. Similarly, we also choose two individual years, the first year, 2003, and the second last year, 2010, to quantify the DLST (note that the last year 2011 is not chosen because of its abnormal LST due to the historic drought in 2011).

As the DLST also contains the background "regional interannual variability" signal at these two periods (or years) that is unrelated to wind farms, we subtract this signal from the original anomalies for each pixel (referred to as "pixel level anomaly") to minimize its impact on DLST (Zhou et al. 2012). Doing so emphasizes the DLST spatial variability at pixel scale. For example, if a region is warmer this year than last year but with different warming rates at different pixels, the DLST (this year's anomaly minus last year's anomaly) will show the warming everywhere, but after removing the regional mean warming rate, the spatial variability of the warming rate for every pixel can be easily identified. Note that the "pixel level anomaly" represents relative changes, not the absolute changes. In other words, the resulting warming or cooling rate represents a change relative to the regional mean value. Note

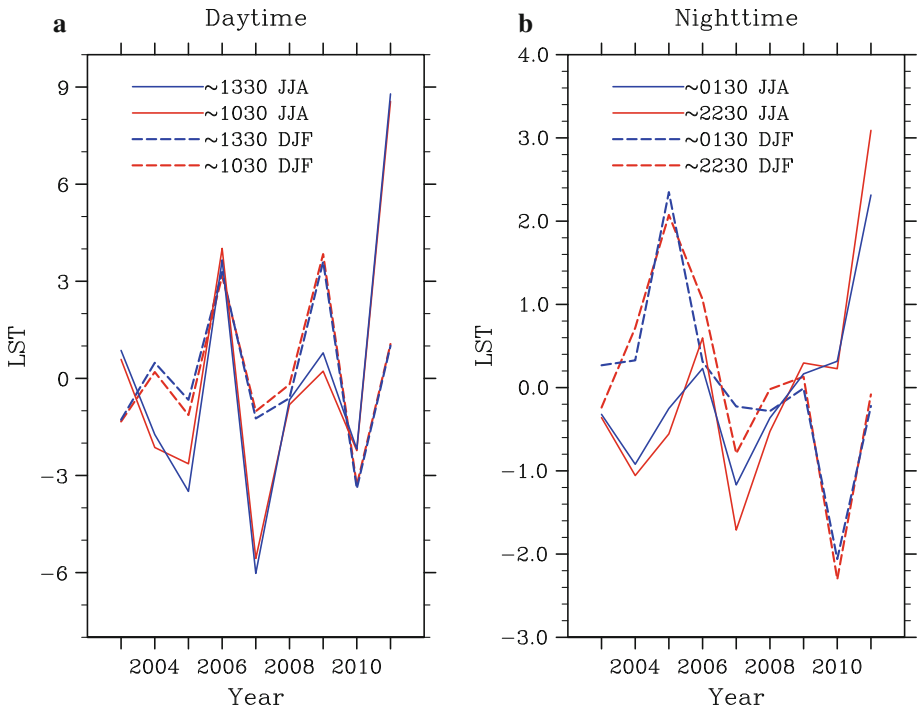

Fig. 4 Interannual variations of regional mean anomalies of MODIS LST (°C) in DJF and JJA at **a** daytime and **b** nighttime averaged over the study region for the period 2003–2011

that Method I is used primarily to examine the spatial coupling between wind turbines and LST changes, while Method II introduced next is used to quantify the wind farm impacts on LST.

2.5.3 *Quantification of temporal LST changes*

We use the areal mean LST differences between WFPs and NNWFPs (WFPs minus NNWFPs), denoted as ΔLST, for each year to quantify the impacts of wind farms on LST for the period of 2003–2011 (referred to as Method II). The areal mean LST changes instead of the pixel level LST changes is considered here as spatial averaging is commonly used to reduce satellite data noise and uncertainties. Method II has been extensively used to estimate urban heat island effects by comparing observed temperatures in urban stations with their nearby rural ones (Gallo and Owen 1997; Peterson 2003). It assumes that the urban and rural stations share the same large-scale weather conditions and thus their differences are due primarily to local urban effects. Unlike Method I, Method II does not explicitly remove the regional interannual variability but implicitly performs the same function. It should be realized that WFPs and NNWFPs may differ in their land surface properties (e.g., elevation and land cover types) and thus ΔLST also contains the LST spatial variation due to this difference. However, Method II examines how the ΔLST changes temporally with the development of wind farms while the land surface properties do not change much with time over NNWFPs (Zhou et al. 2012). Simply put, we examine how the LSTs between two fixed groups of pixels change from 2003 to 2011 with unchanged land surface properties in one group.

There are various ways to quantify temperature changes with time. Here we use two different methods as described in Wigley and Santer (2012). First, we simply calculate the ΔLST difference between two periods (2009–2011 minus 2003–2005 averages) or two individual years (2010 minus 2003) as done in Method I and define this difference as "the total change" (referred to as Method II-A). Second, we estimate the least-squares linear trend of ΔLST over the study period as done in Zhou et al. (2012) and define "the total trend" as the trend per year multiplied by the interval in years over which the trend is calculated (referred to as Method II-B). Method II-A is straightforward but may not be a good indicator because LST shows strong interannual variations and is particularly noisy at daytime. Although there are only 9 years of data, Method II-B can be used as another good indicator because the number of operational wind turbines has increased steadily with time since 2003 and our analysis shows in the next section persistent upward trends in LST at nighttime. Furthermore, it can provide the p value of t-statistics that quantify the probability of whether the trend is statistically significant from zero or simply due to random noise. Therefore, the total change is more meaningful to represent the LST change if there is a statistically significant trend in the data. In addition, the temporal LST

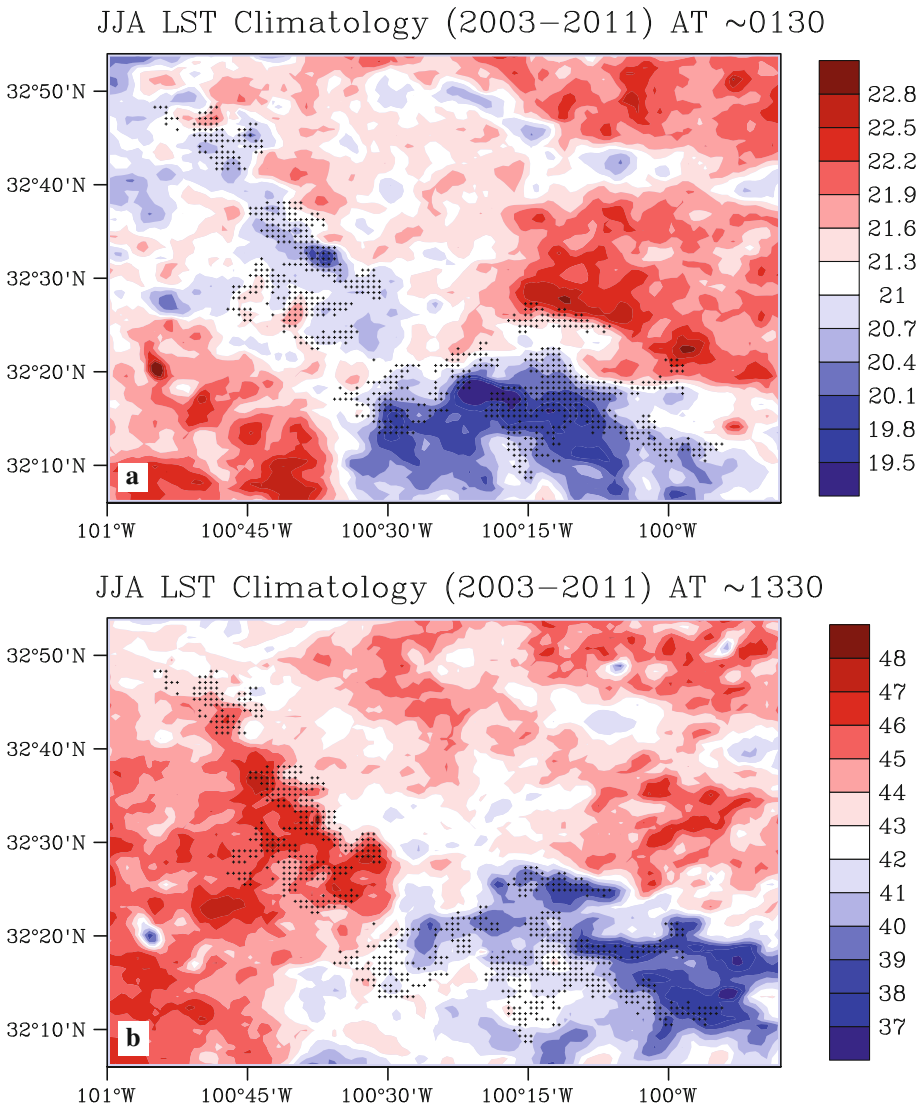

Fig. 5 MODIS JJA LST climatology (°C) (2003–2011 averages) at **a** nighttime ~01:30 and **b** daytime ~13:30. *Pixels* with *plus symbol* have at least one wind turbine (i.e., WFPs)

Table 4 Seasonal statistics of climatological MODIS LSTs (°C) for WFPs and NNWFPs (in parenthesis) for the period 2003–2011

Season	Nighttime		Daytime	
	~22:30	~01:30	~10:30	~13:30
DJF	2.98 (2.71)	1.39 (1.37)	17.20 (17.44)	20.96 (21.27)
MAM	13.21 (13.47)	11.24 (11.65)	32.23 (32.40)	35.63 (35.78)
JJA	22.27 (22.75)	20.73 (21.31)	39.33 (39.65)	42.59 (43.16)
SON	12.69 (12.74)	11.15 (11.18)	27.44 (27.88)	30.14 (30.81)
ANN	12.79 (12.91)	11.12 (11.37)	29.04 (29.33)	32.32 (32.75)

WFPs and NNWFPs are defined in Fig. 2c; the values shown are the climatology of areal mean LSTs for WFPs and NNWFPs, respectively

changes estimated from Method II-A and -B may be sensitive to the abnormal LST in 2011 which has nothing to do with the wind farms. So we also have to consider the ΔLST changes by including and excluding the data in 2011 in our analysis. Nevertheless, the results from these two methods should be consistent if there are noticeable impacts from wind farms.

3 Results

3.1 Spatial coupling between wind turbines and LST changes

Figure 6 shows the "pixel level anomaly" differences of ANN LST between the averages of 2009–2011 and those of

2003–2005 using Method I. The nighttime LSTs at ~22:30 and ~1:30 demonstrate similar features: (a) WFPs are generally much warmer than NNWFPs; (b) the warming is also observed in downwind pixels of wind turbines (the prevailing wind is from south, Fig. 3); (c) there is a spatial coupling between the wind turbines and the warming over most WFPs. The daytime LSTs at ~10:30 and ~13:30 show a small and much noisy warming effect over some WFPs but overall there is no spatial coupling between the wind turbines and the LST change. Figure 7 shows the nighttime LST changes in DJF and JJA. Evidently, the warming effect over WFPs is visible in both seasons but better coupled with the wind turbines and less noisy in summer than winter.

Figure 8 shows the MODIS JJA nighttime LST "pixel level anomaly" differences between 2010 and 2003. Evidently, it exhibits similar features as Fig. 7 but with a much larger magnitude, which is expected as it is from a single year while the latter are from three-year averages. The spatial coupling between the wind farms and the warming areas is very strong. After examining the spatial patterns of LST changes at nighttime in other seasons (figures not shown), we find that this spatial coupling is strongest in JJA, followed by SON, and is weakest (or noisiest) in DJF and MAM.

Figure 9 shows the box-and-whisker diagram of nighttime LST differences between the averages of 2009–2011 and those of 2003–2005 and between 2010 and 2003 in all seasons. Evidently, the 25th percentile, median, 75th percentile LSTs in WFPs are always larger than those in NNWFPs, suggesting a warming effect over WFPs relative to NNWFPs, and this warming is the strongest in JJA, particularly at ~22:30.

3.2 LST temporal changes

Figure 10 shows the total trends and their significance levels for the ΔLST time series anomaly in DJF and JJA for the period of 2003–2011. While the time series is short, the ΔLST exhibits apparent upward trends at nighttime. We have identified statistically significant warming trends of 0.31 °C/8 years ($p = 0.0098$) at ~1:30 and 0.45 °C/8 years ($p = 0.0004$) at ~22:30 in DJF and 0.48 °C/8 years ($p = 0.0338$) at ~01:30 and 0.67 °C/8 years ($p = 0.0003$) at ~22:30 in JJA. At daytime, the LST displays strong interannual variations and all the trends are statistically insignificant at the 5 % level, suggesting that the changes are random.

We performed the same analysis for all other seasons as done in Fig. 10 and list all of the total trends in Tables 5, 6 (QA0). The nighttime LST trends in all seasons, except ~1:30 in MAM, are statistically significant ($p < 0.01$ at ~22:30 and $p < 0.05$ at ~1:30), with a total trend of 0.31–0.67 °C for the period of 2003–2011 and of 0.34–0.70 °C for the period of 2003–2010. Among the four seasons, the warming trend is strongest in JJA, followed mostly by SON, and smallest in DJF and MAM. For the two MODIS measurements at nighttime, ~22:30 has stronger warming rates and also higher significance levels than ~1:30. In contrast, the daytime trends range from negative to positive values and none is statistically significant at the 5 % level. It is interesting to note that unlike other daytime trends, the LST in DJF at ~10:30 shows a total trend of 0.36–0.40 °C that is statistically significant at the 10 % level.

Table 7 (QA0) lists the total change between two periods: 2011–2009 minus 2003–2005 averages and 2010 minus 2003 (in parenthesis) for all seasons. The nighttime LST increases with time in all seasons and for both periods. The total changes are 0.28–0.51 °C for the period of 2003–2011 and 0.26–0.74 °C for the period of 2003–2010. Among the four seasons, the increase is strongest in JJA. For the two MODIS nighttime measurements, ~22:30 has a larger increase than ~1:30. Again, the daytime LST shows "positive" and "negative" changes. These results are generally consistent with the total trends listed in Tables 5, 6.

3.3 LST temporal changes under different QA controls

Table 2 lists the percentage of LST retrievals under different QA controls for WFPs and NNWFPs. For QA0, the MODIS LSTs are retrieved from 93.6 to 99.9 % (92.1–99.8 %) of the pixels at nighttime (daytime); for the two nighttime measurements, ~22:30 has a slightly higher retrieval percentage than ~1:30; among the four seasons, the LST has a lower retrieval rate at ~1:30 and ~13:30 in JJA than other seasons. So the overall retrieval percentage for QA0 are very high, indicating that only a few pixels are not retrieved by MODIS due to cloud effects or other factors. This is probably because the study region, which is located between the semi-arid West Texas and the subtropical sub-humid Central Texas, is mostly cloud free. The record from a nearby weather station in Abilene, TX, shows that the study region receives plentiful sunshine (Combs 2008b). QA1 represents the best quality with a retrieval percentage of 62.4–70.4 % for all seasons and acquisition times except for a lower retrieval rate of 37.0–49.3 % at ~1:30 and ~13:30 in JJA. QA2 shows similar features as QA1 but has a much higher retrieval rate of 81.6–94.6 % at nighttime and 77.3–89.2 % at daytime except for a lower retrieval rate of 46.1–63.6 % at ~1:30 and ~13:30 in JJA. QA3 exhibits almost identical results as QA0. For the four QA controls, on average, the retrievals at nighttime are much higher than those at daytime, with the highest rate at ~22:30. The lowest retrieval rate is observed at ~13:30 in JJA and followed by ~1:30 in JJA.

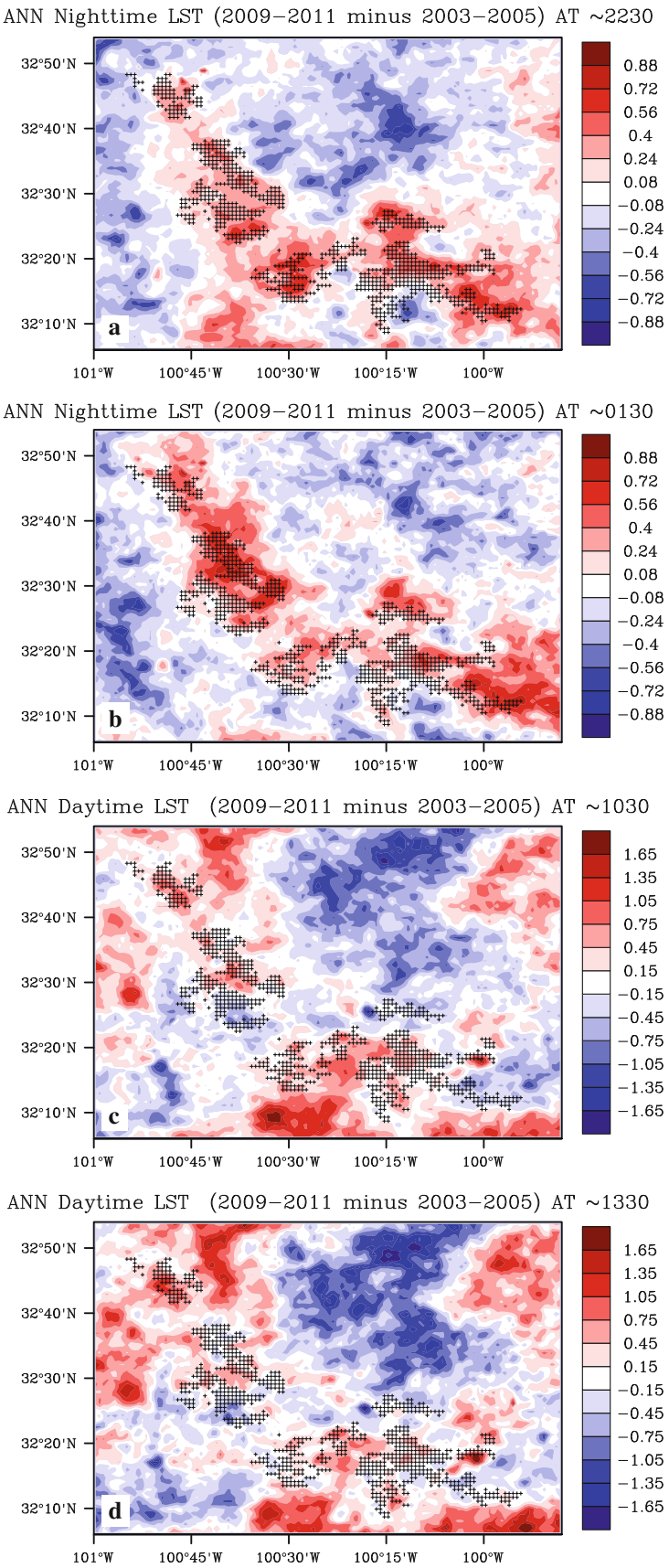

Fig. 6 Annual mean LST differences (°C) (2009–2011 minus 2003–2005 averages) at **a**, **b** nighttime and **c**, **d** daytime. *Pixels* with *plus symbol* have at least one wind turbine (i.e., WFPs)

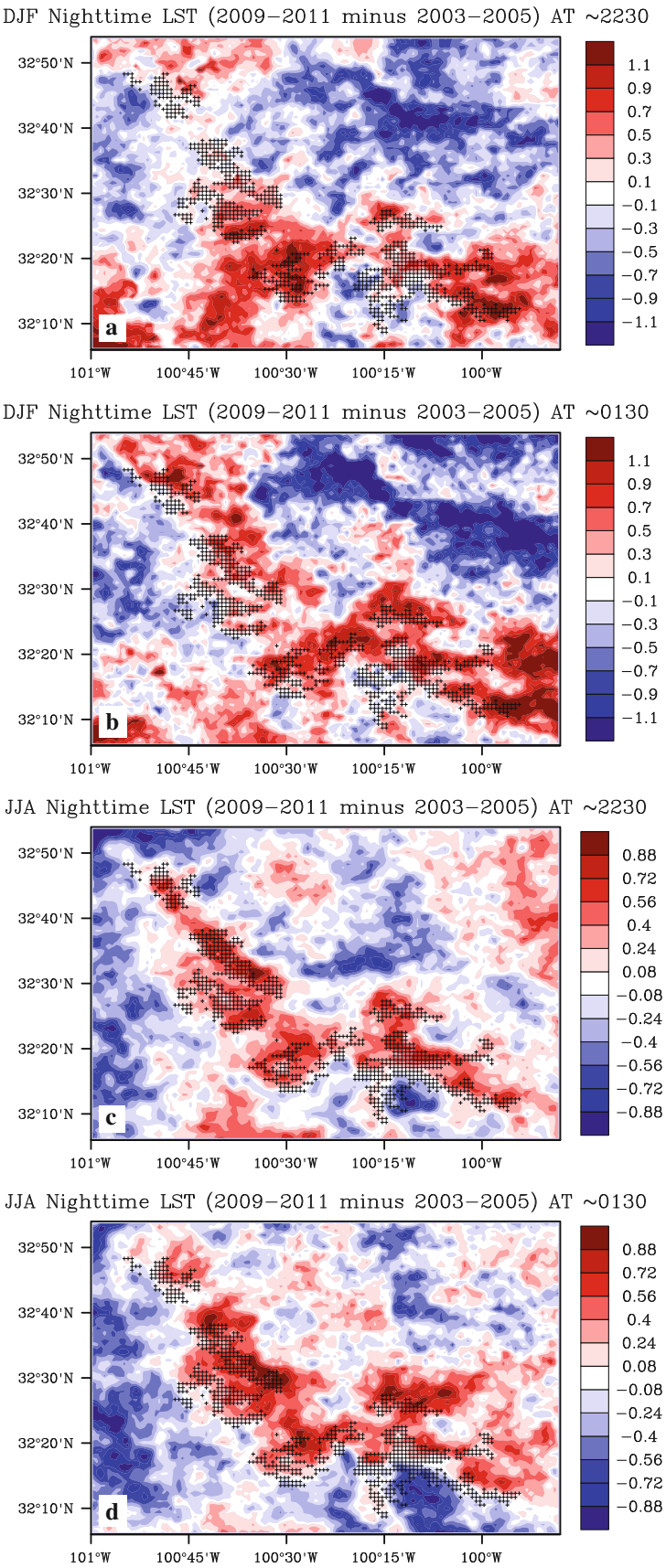

Fig. 7 DJF and JJA nighttime LST differences (°C) (2009–2011 minus 2003–2005 averages) at ~22:30 (**a**, **c**) and ~01:30 (**b**, **d**). *Pixels* with *plus symbol* have at least one wind turbine (i.e., WFPs)

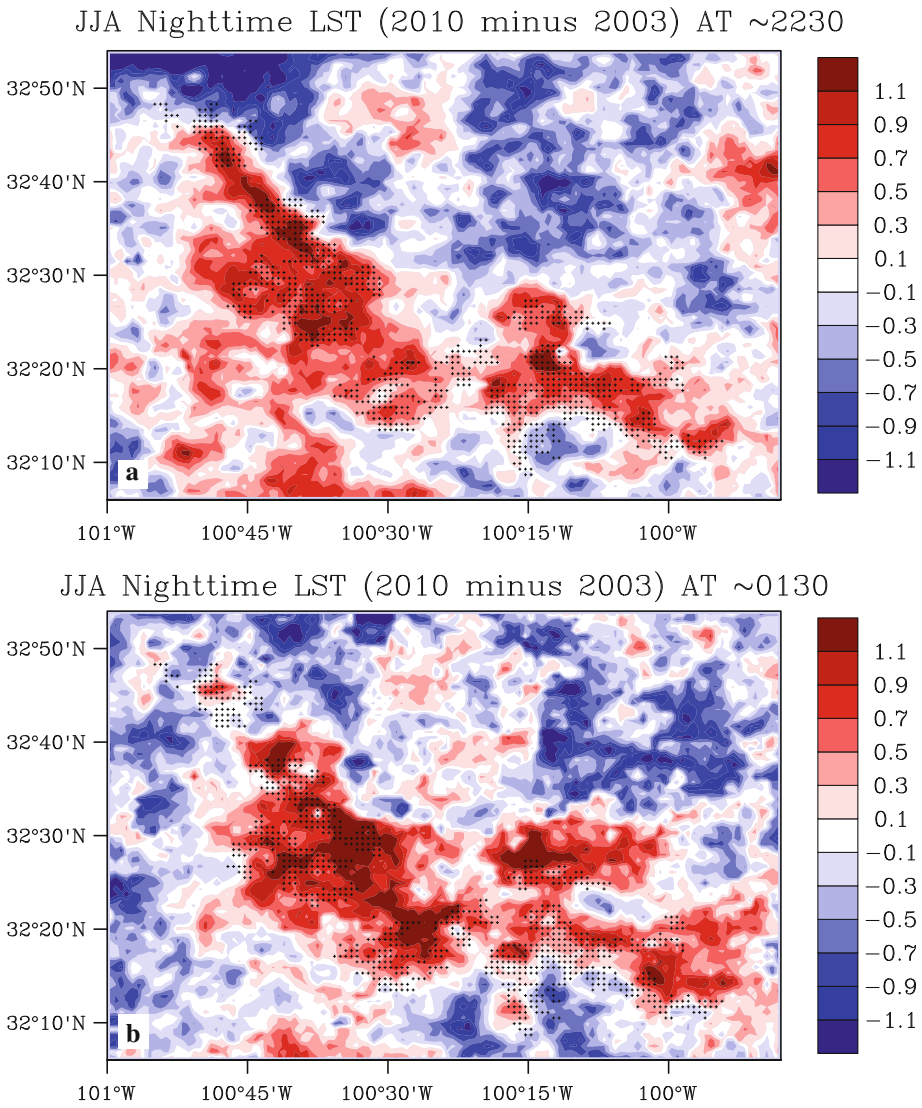

Fig. 8 JJA nighttime LST differences (°C) (2010 minus 2003) at **a** ~22:30 and **b** ~01:30. *Pixels* with *plus symbol* have at least one wind turbine (i.e., WFPs)

The aforementioned results in Sects. 3.1 and 3.2 correspond to the QA control for QA0. The total trends (Tables 5, 6) and the total changes (Table 7) under other QA controls give consistent results: (1) the daytime LST shows statistically insignificant total trends or very noisy total changes except DJF at ~10:30; (2) the nighttime LST shows warming trends that are all statistically significant at the 5 % level or consistent increases in the total change; (3) this warming effect is stronger and better coupled with wind farms at nighttime than daytime in all seasons and at ~22:30 than ~1:30. The magnitude of the warming of QA1, QA2 and QA3 is slightly smaller than that of QA0. For example, the total trend (Tables 5, 6) at ~22:30 in JJA is 0.67 °C ($p < 0.001$) in QA0, 0.59 °C ($p = 0.001$) in QA1, 0.62 °C ($p < 0.001$) in QA1, and 0.67 °C ($p < 0.01$) in QA2 for the period of 2003–2011. The corresponding total change (Table 7) is 0.51 °C (0.74 °C), 0.46 °C (0.70 °C), 0.47 °C (0.75 °C) and 0.51 °C (0.74 °C) for the LST of 2011–2009 minus 2003–2005 averages (2010 minus 2003).

In addition, we also assess uncertainties of our results due to the differences in defining NNWFPs. NNWFPS refers to those non wind farm pixels that are very close to WFPs but not affected by wind farms. Obviously, it can be defined otherwise. Delineating pixels with and without wind farm impacts is not easy given the difficulties in objectively defining the boundary of downwind pixels of wind farms. Also wind direction changes with time. One simple way is to define all of the non wind farm pixels as NNWFPs and recalculate the total trend and total change as done previously. The results (not shown) differ slightly in magnitude from but are essentially similar to those listed in Tables 5, 6, 7.

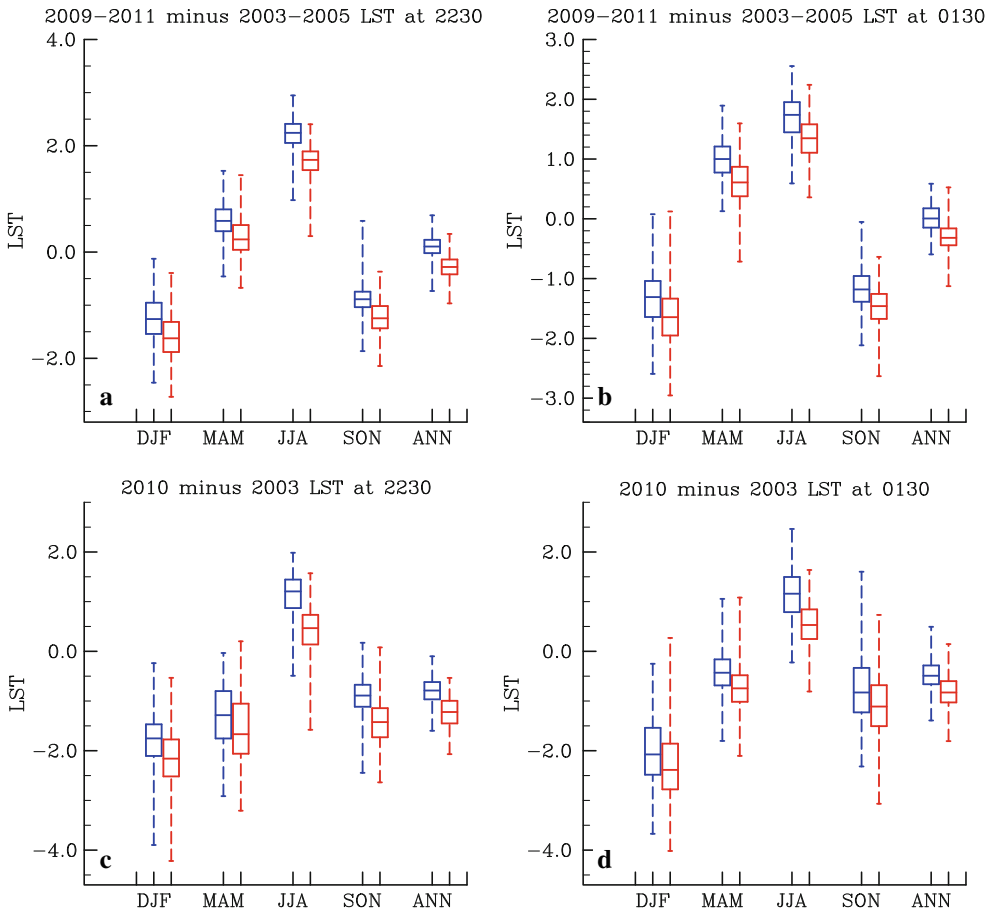

Fig. 9 Box-and-whisker diagram of seasonal mean nighttime LST differences (°C): 2009–2011 minus 2003–2005 averages (**a**, **b**) and 2010 minus 2003 (**c**, **d**) at ~22:30 and ~01:30 over WFPs and NNWFPs respectively. Each *box* is used to depict groups of the LST differences from WFPs (in *blue*) or NNWFPs (in *red*) through their five values: the minimum, 25th percentile, median, 75th percentile, and maximum LST. The *bottom* and *top* of the *box* are the 25th and 75th percentile (the lower and upper quartiles, respectively), and the band near the middle of the box is the median. WFPs and NNWFPs are defined as in Fig. 2c

4 Discussion and conclusions

The above results indicate that there is a warming effect seen by MODIS at nighttime coupled with the wind farms over the study region. In terms of the magnitude of the nighttime warming, the total trend is estimated between 0.31–0.67 °C for the period of 2003–2011 and 0.34–0.70 °C for the period of 2003–2010, and the corresponding total change is between 0.28–0.51 °C and 0.26–0.74 °C respectively. Among the four seasons, the warming effect is strongest in JJA, followed mostly by SON, and smallest in DJF and MAM. For the two MODIS measurements at nighttime, the warming effect is stronger at ~22:30 than ~1:30. Consequently, the largest warming effect is observed at ~22:30 in JJA. These results remain robust under different quality controls and using different methods in quantifying the LST changes.

Can this warming be attributable to the development of wind farms? Zhou et al. (2012) have discussed and examined possible contributors, e.g., incoming surface radiation, land surface properties, elevation and land use, and found that the diurnal and seasonal variations in wind speed and the changes in near-surface atmospheric boundary layer (ABL) conditions due to wind farm operations are likely the primary causes. Here we discuss this attribution further with more analysis.

The seasonal and diurnal variations of wind speed should play a key role in explaining the above LST changes because wind speed is the primary variable that determines the amount of power generated by wind turbines. Zhou et al. (2012) used monthly mean wind data to simply calculate the wind speed mean and standard deviation (STD) and found that the wind is stronger at nighttime than daytime and much stronger in summer than winter. However, they underestimated the instantaneous wind speed because the winds of opposite directions are smoothed out in the monthly mean data.

Three key wind variables are often used to estimate wind power generation: (1) cut-in speed—the minimum

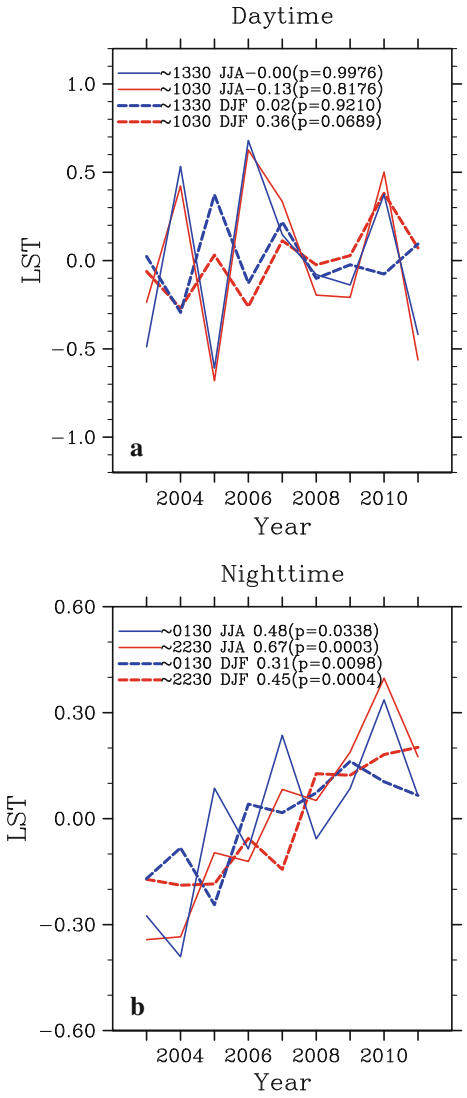

Fig. 10 Interannual variations in areal mean LST (°C) differences between WFPs and NNWFPs (WFPs minus NNWFPs) at daytime ~10:30 and ~13:30 and nighttime ~22:30 and ~01:30 in DJF and JJA for the period 2003–2011. The total trends (°C) and significance levels (*p* values) are shown. The total trend is calculated as the linear trend per year estimated using least squares fitting multiplied by the interval in years (i.e., 8 years). The *p* value tells the probability of whether the linear trend value is statistically significantly different from zero. WFPs and NNWFPs are defined as in Fig. 2c

wind speed at which the turbine begins to rotate, typically 3–4 m/s, (2) rated-output speed—the wind speed at which the power output reaches the upper limit of the generator, typically 12–17 m/s, and (c) cut-out speed—the maximum wind speed at which the turbine stops as a safety feature to protect the turbine from damage, typically around 25 m/s. For the wind speed between the cut-in speed and rated-output speed, the power output of a wind generator is proportional to the cube of the wind speed—i.e., a doubling of the wind speed will increase the power output by a factor of 8. Therefore, the wind speed frequency distribution is a more scientifically reasonable parameter to estimate the power generation than the simple statistics used in Zhou et al. (2012).

Table 3 lists the climatological statistics of 50 m wind speed and STD over our study region for the period of 2003–2011. Among the four seasons, the wind speed varies between 6.99–8.19 w/s at nighttime and 5.08–6.88 m/s at daytime, with the strongest values observed in MAM. For all four MODIS measuring times, wind speed is much larger at nighttime than daytime and this day-night difference peaks up to 2.12 m/s in JJA. During the nighttime, the wind is slightly stronger at ~22:30 than ~1:30 in JJA and SON, while it is slightly weaker at ~22:30 than ~1:30 in DJF and MAM. Overall, the day-night difference is strong and consistent with the statistics in Zhou et al. (2012) while the seasonal difference is much smaller than that in Zhou et al. (2012), which shows that the wind speed in JJA is about twice that in DJF. Unlike the mean values, the STD differs by a large amount between seasons, with the smallest value in JJA, followed by SON, the largest in MAM and DJF, indicating a stronger variation in wind speed in cold seasons than warm seasons.

Figure 3 shows the probability distribution function (PDF) of the wind speed and direction in DJF and JJA. In terms of wind direction, the prevailing wind over the study region is from south, particularly in summer, with an additional peak of northerly wind in winter. Other directions of wind also occur but with a much lower frequency. So the wind direction is stable and dominantly from south in summer but changes more frequently in winter between southerly and northerly winds. In terms of wind speed, the PDF in summer is much narrower and has a higher percentage of wind speed located between the cut-in and rated-output speed range than that in winter and the peak wind speed in summer is also larger than that in winter. At nighttime, ~22:30 has a slightly higher frequency of higher wind speed than ~1:30.

Baidya Roy (2011) estimated the power generation efficiency as a function of wind speed for a Gamesa G80 2.0 MW wind turbine and found that the wind speed of 8 m/s corresponds to the maximum efficiency. Here we simply estimate the percentage of the optimal wind speed range centered at 8 m/s relative to the whole wind spectrum. Table 3 (the second five rows) lists the frequency of wind speed of 7–9 m/s and 6–10 m/s in each season. Evidently, the percentage of the optimal wind speed for power generation is much larger at nighttime than daytime and slightly higher at ~22:30 than at ~1:30. Among the four seasons, the highest is in JJA, followed by SON, and the least in either MAM or DJF. So the average wind speed differs little among seasons but their percentages of the optimal wind speed range vary significantly, with the JJA nighttime being the best for the power generation.

Table 5 Total trends and significance levels (in parenthesis) for MODIS LST differences (°C) between WFPs and NNWFPs for the period 2003–2011

QA type[a]	Season	Nighttime		Daytime	
		~22:30	~01:30	~10:30	~13:30
QA0	DJF	0.45 (<0.001)	0.31 (0.010)	0.36 (0.069)	0.02 (0.921)
	MAM	0.39 (0.003)	0.51 (0.060)	−0.13 (0.710)	−0.00 (0.996)
	JJA	0.67 (<0.001)	0.48 (0.034)	−0.13 (0.818)	−0.00 (0.998)
	SON	0.47 (0.005)	0.43 (0.016)	−0.11 (0.735)	−0.16 (0.643)
	ANN	0.50 (<0.001)	0.42 (0.007)	−0.01 (0.942)	−0.06 (0.774)
QA1	DJF	0.21 (0.023)	0.26 (0.151)	0.57 (0.071)	−0.17 (0.577)
	MAM	0.33 (0.007)	0.40 (0.054)	−0.06 (0.871)	0.21 (0.533)
	JJA	0.59 (0.001)	0.35 (0.069)	−0.51 (0.483)	0.48 (0.570)
	SON	0.56 (0.001)	0.48 (0.016)	−0.01 (0.968)	−0.06 (0.870)
	ANN	0.38 (0.001)	0.26 (0.025)	−0.04 (0.844)	0.12 (0.563)
QA2	DJF	0.27 (0.020)	0.29 (0.098)	0.62 (0.050)	−0.16 (0.580)
	MAM	0.36 (0.013)	0.43 (0.042)	−0.12 (0.696)	0.16 (0.650)
	JJA	0.62 (<0.001)	0.42 (0.021)	−0.29 (0.702)	0.60 (0.497)
	SON	0.46 (0.005)	0.47 (0.024)	0.03 (0.938)	−0.03 (0.944)
	ANN	0.43 (<0.001)	0.40 (0.002)	0.05 (0.821)	0.09 (0.734)
QA3	DJF	0.45 (<0.001)	0.31 (0.010)	0.36 (0.069)	0.02 (0.913)
	MAM	0.39 (0.003)	0.51 (0.060)	−0.13 (0.710)	−0.00 (0.996)
	JJA	0.67 (<0.001)	0.47 (0.034)	−0.12 (0.827)	0.02 (0.974)
	SON	0.47 (0.005)	0.43 (0.016)	−0.11 (0.735)	−0.16 (0.643)
	ANN	0.50 (<0.001)	0.42 (0.007)	−0.01 (0.949)	−0.05 (0.794)

WFPs and NNWFPs are defined in Fig. 2c; the total trend is calculated as the linear trend per year multiplied by the interval in years (i.e., 8 years)

[a] QA types are defined as in Table 2

The seasonal difference in the warming effect might be also related to the wind turbine wake effect. As the turbines in our study region are structured in rows along the southeastern direction to maximize the use of dominant southerly wind, the turbine spacing is larger in the north–south direction than the west–east direction and consequently the turbine wake effect is stronger for the zonal winds than the meridional ones. Table 3 (the last five rows) shows the frequency of wind direction within an angle of ±7.5° and ±15° along the west-east direction. Evidently, JJA and SON have a much lower frequency of zonal winds than MAM and DJF. So the presence of wind directions other than northerly and southerly in winter and other transitional seasons may also reduce, to some extent, the efficiency of wind power generation.

Therefore, the stronger wind speed at nighttime than daytime and the higher frequency of the wind speed within the optimal power generation range in JJA than DJF likely drive wind turbines to generate more electricity and turbulence and consequently results in the strongest warming effect at nighttime in JJA. Similarly, the stronger wind speed and the higher frequency of optimal wind speed at ~22:30 than that at ~1:30 might help explain, to some extent, why the nighttime LST warming effect is slightly larger at ~22:30 than ~1:30.

Changes in near-surface ABL conditions due to wind farm operations should be also responsible for the LST warming observed in MODIS data (Zhou et al. 2012). The nocturnal ABL is typically stable and much thinner than the daytime ABL and hence the turbine enhanced vertical mixing produces a stronger nighttime effect (Eastman et al. 2001; McNider et al. 2005; Pielke and Matsui 2005; Kumar et al. 2010). It is expected that the enhanced vertical mixing in the wakes generated by wind turbine rotors will create a warming (cooling) effect at nighttime (daytime) by pulling down warmer (colder) near surface air from higher altitudes. However, daytime mixing is already very large due to solar heating. Hence, the turbine-enhanced turbulent mixing may play a smaller role during the daytime as shown above. Zhou et al. (2012) speculate that the slow development of the unstable layer at daytime (Stull 2009) might help explain the weak daytime warming seen over some WFPs. As discussed in Sect. 3.2, the daytime LST at ~10:30 show a warming effect in DJF (Tables 5, 6, 7) with a total trend of 0.36–0.40 °C ($p < 0.07$), a noticeable feature differing

Table 6 Total trends and significance levels (in parenthesis) for MODIS LST differences (°C) between WFPs and NNWFPs for the period 2003–2010

QA type[a]	Season	Nighttime		Daytime	
		~22:30	~01:30	~10:30	~13:30
QA0	DJF	0.41 (0.002)	0.34 (0.008)	0.40 (0.068)	−0.04 (0.889)
	MAM	0.34 (0.016)	0.52 (0.084)	−0.19 (0.621)	0.03 (0.949)
	JJA	0.70 (<0.001)	0.55 (0.023)	0.26 (0.635)	0.31 (0.577)
	SON	0.52 (0.003)	0.48 (0.012)	−0.13 (0.728)	−0.03 (0.933)
	ANN	0.48 (<0.001)	0.44 (0.009)	0.08 (0.651)	0.07 (0.742)
QA1	DJF	0.16 (0.091)	0.26 (0.212)	0.54 (0.123)	−0.32 (0.341)
	MAM	0.33 (0.014)	0.45 (0.050)	−0.03 (0.946)	0.34 (0.346)
	JJA	0.68 (<0.001)	0.46 (0.020)	−0.05 (0.947)	1.01 (0.257)
	SON	0.63 (<0.001)	0.47 (0.029)	−0.07 (0.861)	−0.01 (0.984)
	ANN	0.38 (0.001)	0.30 (0.014)	0.08 (0.664)	0.26 (0.223)
QA2	DJF	0.25 (0.048)	0.25 (0.186)	0.68 (0.054)	−0.41 (0.149)
	MAM	0.29 (0.052)	0.40 (0.088)	−0.13 (0.708)	0.22 (0.562)
	JJA	0.65 (<0.001)	0.49 (0.009)	0.10 (0.902)	1.09 (0.250)
	SON	0.53 (0.001)	0.51 (0.022)	0.03 (0.948)	0.01 (0.973)
	ANN	0.41 (<0.001)	0.40 (0.005)	0.15 (0.552)	0.20 (0.465)
QA3	DJF	0.41 (0.002)	0.34 (0.008)	0.40 (0.068)	−0.03 (0.898)
	MAM	0.34 (0.016)	0.52 (0.084)	−0.19 (0.621)	0.03 (0.949)
	JJA	0.70 (<0.001)	0.54 (0.023)	0.27 (0.629)	0.34 (0.545)
	SON	0.52 (0.003)	0.48 (0.012)	−0.13 (0.728)	−0.03 (0.933)
	ANN	0.48 (<0.001)	0.44 (0.009)	0.08 (0.645)	0.08 (0.717)

WFPs and NNWFPs are defined in Fig. 2c; the total trend is calculated as the linear trend per year multiplied by the interval in years (i.e., 7 years)

[a] QA types are defined as in Table 2

from all other daytime values. Thus this example is consistent with the speculation of Zhou et al. (2012). In winter, the early morning ABL condition should be closer to that of nighttime than to that of afternoon. Consequently, the stable and thinner ABL at ~10:30 in DJF than other season at the same local solar time may make the warming noticeable. Further attribution, however, requires observational analysis of meteorological variables (e., temperature, humidity and wind profiles) and turbine parameters (e.g., hub-height, rotor diameter, power curve, power generation and downtime) at hourly and higher temporal resolutions over wind farms, much of which are commercial proprietary information and thus are not available in the public domain.

Remote sensing data at spatial resolution finer than inter-turbine space and sampling frequency that can capture the full diurnal cycle of LST and ABL (e.g., hourly) would be most effective to detect impacts of wind farms than MODIS. However, MODIS LST is the only high quality satellite data that are publically available, have a spatial resolution smaller than most big wind farms, and have data for ~10 years covering both day and night times. We realize that the MODIS data do contain errors and noise due to cloud contamination and imperfection of retrieval algorithms (Wan 2006) and thus may result in some biases (e.g., small areas of noticeable warming or cooling appearing randomly in Figs. 6, 7, 8 are difficult to explain). Uncertainties also exist in wind turbine locations (e.g., the builders may relocate their turbine sites slightly from their original filing with FAA) as well as operations (some turbines may be not operating due to damage or repair). However, our use of spatial and temporal averaging should largely remove such errors and uncertainties. The remaining residuals, if any, cannot accidentally create the strong spatial coupling between the warming and wind turbines shown above.

In summary, our results indicate that the warming effect seen in the MODIS data over wind farms are very likely due to the development of wind farms because (a) the spatial pattern of the warming resembles the geographic distribution of wind turbines, (b) the temporal LST changes over WFPs shows a persistent upward trend from 2003 to 2011 relative to NNWFPs, consistent with the increasing number of operational wind turbines with time, (c) the

Table 7 Total changes for MODIS LST differences (°C) between WFPs and NNWFPs for 2011–2009 minus 2003–2005 averages and for 2010 minus 2003 (in parenthesis)

QA type[a]	Season	Nighttime		Daytime	
		~22:30	~01:30	~10:30	~13:30
QA0	DJF	0.35 (0.35)	0.28 (0.27)	0.26 (0.44)	−0.04 (−0.10)
	MAM	0.30 (0.26)	0.38 (0.30)	−0.30 (0.21)	−0.20 (0.45)
	JJA	0.51 (0.74)	0.36 (0.61)	0.07 (0.74)	0.13 (0.86)
	SON	0.34 (0.53)	0.30 (0.35)	−0.10 (0.03)	−0.10 (0.17)
	ANN	0.37 (0.43)	0.31 (0.33)	−0.02 (0.32)	−0.07 (0.36)
QA1	DJF	0.16 (0.05)	0.27 (−0.07)	0.41 (0.68)	−0.20 (−0.41)
	MAM	0.25 (0.30)	0.32 (0.28)	−0.22 (0.23)	0.01 (0.61)
	JJA	0.46 (0.70)	0.24 (0.64)	−0.18 (0.84)	0.52 (2.20)
	SON	0.43 (0.59)	0.37 (0.35)	−0.03 (0.18)	−0.04 (0.05)
	ANN	0.28 (0.31)	0.22 (0.20)	−0.03 (0.42)	0.08 (0.56)
QA2	DJF	0.22 (0.14)	0.27 (−0.07)	0.48 (0.67)	−0.22 (−0.56)
	MAM	0.25 (0.25)	0.30 (0.20)	−0.26 (0.22)	−0.05 (0.67)
	JJA	0.47 (0.75)	0.30 (0.70)	0.02 (0.91)	0.63 (2.31)
	SON	0.36 (0.45)	0.34 (0.43)	−0.00 (0.36)	−0.03 (0.12)
	ANN	0.31 (0.36)	0.30 (0.28)	0.05 (0.51)	0.05 (0.61)
QA3	DJF	0.35 (0.35)	0.28 (0.27)	0.26 (0.44)	−0.03 (−0.10)
	MAM	0.30 (0.26)	0.38 (0.30)	−0.30 (0.21)	−0.20 (0.45)
	JJA	0.51 (0.74)	0.35 (0.61)	0.08 (0.75)	0.14 (0.91)
	SON	0.34 (0.53)	0.30 (0.35)	−0.10 (0.03)	−0.10 (0.17)
	ANN	0.37 (0.43)	0.31 (0.33)	−0.02 (0.33)	−0.06 (0.37)

WFPs and NNWFPs are defined in Fig. 2c; the total change is calculated as the areal mean LST difference (NWPs minus NNWFPs) between the two periods

[a] QA types are defined as in Table 2

seasonal and diurnal variations in the ABL conditions and the frequency of wind speed and direction distribution are consistent with those in the observed warming effect. Furthermore, these results remain robust under different quality controls and using different methods in quantifying the temporal LST changes.

Because this analysis is from a short period over a region with rapid growth of wind farms, we expect our estimates to give higher values than those estimated in other locations and over longer periods. The use of linear trends here is just one simple way to quantify the wind farm impacts while reducing the data uncertainties and noise. It is important to note that the estimated warming trends only apply to the study region and to the study period, and thus should not be extrapolated linearly into other regions or over longer periods (e.g., for another 20 years). For a given wind farm, once there are no new wind turbines added, the warming effect may reach a stable level (when comparing the case without wind farms). In addition, other factors may also modify local LSTs. We will continue our analyses to further our understanding of physical processes and mechanisms of interactions of wind turbines and ABL and thus their effects on weather and climate.

It is important to keep the following points in mind when interpreting our results in terms of their broader implications. First, LST measures the temperature of the Earth's surface and thus has a stronger day-night variation than the surface air temperature from daily weather reports. Therefore, the impacts of wind farms on the surface air temperature should be within the near-surface boundary layer and smaller than the warming signal presented here. Second, the overall warming effect reported in this study is local and is small compared to the strong background year-to-year LST changes. Third, very likely, the wind turbines do not create a net warming of the air and instead only redistribute the heat between different heights in the atmosphere (the turbine itself does not generate any heat), which is fundamentally different from the large-scale warming effect caused by increasing atmospheric concentrations of greenhouse gases due to the burning of fossil fuels. Fourth, generating wind power creates no emissions, uses no water, and is likely green. Wind power is going to be a part of the solution to the climate change, air pollution and energy security problem. Therefore, understanding the wind farm impacts is critical for developing efficient adaptation and management strategies to ensure long-term sustainability of wind power.

Acknowledgments This study was supported by the startup funds provided by University at Albany, SUNY and by National Science Foundation (NSF AGS-1247137). H. Chen was supported by the National Basic Research Program of China (Grant No. 2011CB952000). Y. Dai was supported by the National Natural Science Foundation of China under grant 40875062 and the 111 Project of Ministry of Education and State Administration for Foreign Experts Affairs of China. The MERRA reanalysis data is obtained from the NASA/GSFC/GMAO data server. Chad Eilering and Maxwell Smith helped generate the Google Earth kml files.

References

Adams AS, Keith DW (2007) Wind energy and climate: modeling the atmospheric impacts of wind energy turbines. EOS Trans AGU 88 (Fall Meeting Suppl.), abstr. B44B-08

AWEA (2011) U.S. Wind Energy Market Update, American Wind Energy Association. (http://www.awea.org/learnabout/publications/factsheets/upload/Market-Update-Factsheet-Final_April-2011.pdf)

AWEA (2012) AWEA 4th Quarter 2011 Public Market Report, American Wind Energy Association. (http://awea.org/learnabout/publications/reports/upload/4Q-2011-AWEA-Public-Market-Report_1-31.pdf)

Baidya Roy S (2011) Simulating impacts of wind farms on local hydrometeorology. J Wind Eng Ind Aerodyn. doi:10.1016/j.jweia.2010.12.013

Baidya Roy S, Traiteur JJ (2010) Impacts of wind farms on surface air temperatures. Proc Natl Acad Sci USA 107:17899–17904

Baidya Roy S, Pacala SW, Walko RL (2004) Can large scale wind farms affect local meteorology? J Geophys Res 109:D19101

Barrie D, Kirk-Davidoff D (2010) Weather response to management of large wind turbine array. Atmos Chem Phys 10:769–775

Combs S (2008a) The Energy Report 2008, Texas controller of public accounts. (http://www.window.state.tx.us/specialrpt/energy/)

Combs S (2008b) Texas renewable energy resource assessment, Texas controller of public accounts. (http://www.seco.cpa.state.tx.us/publications/renewenergy/)

Eastman JL, Coughenour MB, Pielke RA (2001) The effects of CO_2 and landscape change using a coupled plant and meteorological model. Glob Change Biol 7:797–815

Fiedler BH, Bukovsky MS (2011) The effect of a giant wind farm on precipitation in a regional climate model. Environ Res Lett 6. doi:10.1088/1748-9326/6/4/045101

Gallo KP, Owen TK (1997) Satellite-based adjustments for the urban heat island temperature bias. J Appl Meteorol 36:1117–1132

Hylton H (2011) Forget irene: the drought in Texas is the catastrophe that could really hurt, Time U.S., 31 Aug 2011. (http://www.time.com/time/nation/article/0,8599,2091192,00.html)

Keith D, DeCarolis J, Denkenberger D, Lenschow D, Malyshev S, Pacala S, Rasch PJ (2004) The influence of large-scale wind power on global climate. Proc Natl Acad Sci USA 101:16115–16120

Kirk-Davidoff DB, Keith DW (2008) On the climate impact of surface roughness anomalies. J Atmos Sci 65:2215–2234

Knippertz P, Ulbrich U, Speth P (2000) Changing cyclones and surface wind speeds over the North Atlantic and Europe in a transient GHG experiment. Clim Res 15:109–122

Kumar V, Svensson G, Holtslag AA, Meneveau C, Parlange MB (2010) Impact of surface flux formulations and geostrophic forcing on large eddy simulations of diurnal atmospheric boundary layer flow. J Appl Meteorol Climatol 49:1496–1516

McNider RT, Lapenta WM, Biazar A, Jedlovec G, Suggs R, Pleim J (2005) Retrieval of gridscale heat capacity using geostationary satellite products: part I: case-study application. J Appl Meteorol 88:1346–1360

Peterson TC (2003) Assessment of urban versus rural in situ surface temperatures in the contiguous United States: no difference found. J Clim 16(18):2941–2959

Pielke RA Sr, Matsui T (2005) Should light wind and windy nights have the same temperature trends at individual levels even if the boundary layer averaged heat content change is the same? Geophys Res Lett 32:L21813. doi:10.1029/2005GL024407

Rienecker M et al (2011) MERRA: NASA's modern-era retrospective analysis for research and applications. J Clim 24:3624–3648

Simmonds I, Keay K (2002) Surface fluxes of momentum and mechanical energy over the North Pacific and North Atlantic Oceans. Meteorol Atmos Phys 80:1–18

Sta Maria MRV, Jacobson MZ (2009) Investigating the effect of large wind farms on energy in the atmosphere. Energies 2(4):816–838

Stull RB (2009) An introduction to boundary layer meteorology. Springer, Berlin, pp 9–19

USDOE (2008) 20 % Wind by 2030, U.S. Department of Energy. (http://www1.eere.energy.gov/wind/pdfs/42864.pdf)

USDOE (2011) Strengthening America's energy security with offshore wind. U.S. Department of Energy. February 2011. (www.nrel.gov/docs/fy11osti/49222.pdf)

Wan Z (2002) Estimate of noise and systematic error in early thermal infrared data of the Moderate Resolution Imaging Spectroradiometer (MODIS). Remote Sens Environ 80:47–54

Wan Z (2006) New refinements and validation of the MODIS land surface temperature/emissivity products. Remote Sens Environ 112:59–74

Wang C, Prinn RJ (2010) Potential climatic impacts and reliability of very large-scale wind farms. Atmos Chem Phys 10:2053–2061

Wigley TML, Santer BD (2012) A probabilistic quantification of the anthropogenic component of 20th century global warming, Clim Dyn (in press)

Zhou L, Tian Y, Baidya Roy S, Thorncroft C, Bosart LF, Hu Y (2012) Impacts of wind farms on land surface temperature. Nat Clim Chang 2(7):539–543